IEEE Access
Multidisciplinary | Rapid Review | Open Access Journal

Received November 4, 2021, accepted December 25, 2021, date of publication January 4, 2022, date of current version January 20, 2022.

Digital Object Identifier 10.1109/ACCESS.2021.3140122

Frequency-Locked Loop Based on Active Noise Cancellation Syncretized Two First-Order Low Pass Filters

LEI PAN, ZHEN LI, JINGMEI ZHANG, AND YI PANG
School of Control and Mechanical Engineering, Tianjin Chengjian University, Tianjin 300384, China
Corresponding author: Jingmei Zhang (meizijingjing@163.com)

ABSTRACT To improve the performance of the frequency lock loop (FLL) under the conditions of a distorted power grid and unexpected noise, a new type of frequency locked loop (Al-FLL) is proposed, in which the AL-FLL prefilter is formed by fusing two first-order low-pass filters (LPFs) with an improved active noise cancellation (ANC) method. Firstly, the improved S function variable step size least mean square algorithm (I-SVSLMS) is discussed and its performance is verified under different signal to noise ratio conditions. Secondly, the function and parameter selection method of LPFs are described. Finally, the stability of the whole system is analyzed. In addition, the denoising work is completed in the synchronous reference frame and the output frequency of the FLL is fed back to the Park transform as the rotation frequency, which further improves the dynamic response and steady state performance of the FLL. The results of simulation and experiment verify the effectiveness and reliability of the proposed method. Compared with the FLL based on second-order generalized integrator (SOGI-FLL), the Comb Filter based on FLL (COMB-FLL), and the AL-FLL without frequency feedback (AL-NF-FLL), the AL-FLL has the advantages of small computation, fast response speed, and small steady-state errors, etc., and it is fully competent to work under the conditions of power grid distortion and unexpected noise.

INDEX TERMS Frequency-locked loop, grid synchronization, active noise cancellation, low pass filter.

I. INTRODUCTION

Signal synchronization is a key factor in the control of power electronic devices, so the accurate detection of voltage signal frequency and phase in the grid synchronization is essential [1], such as the three-phase grid inverter [2], shunt active power filter [3], and island detection [4], etc. Phase locked loop (PLL) and frequency locked loop (FLL) have become the most common methods for grid synchronization due to their simplicity and reliability [5].

The conventional FLL/PLL can determine the signal frequency and phase accurately and quickly under normal conditions. However, when power grid distortion occurs, especially harmonic pollution and three-phase imbalance, the negative sequence component will increase the frequency and phase error of FLL/PLL, making it unable to meet the requirements of grid connection. Thus, many improved PLLs [6]–[8] and FLLs [9]–[13] have been proposed. The most common implementation of PLL is in the synchronous reference frame (SRF), such as SRF-PLL with additional low-pass filter (LSRF-PLL) [6], the PLL with the moving average filter (MAF-PLL) [7] and the cascaded delayed signal cancellation (CDSC-PLL) [8]. These modified PLLs are based on the traditional PLL with a prefilter. The essence of these prefilters is to play the role of low-pass filtering, but the dynamic response of the PLL is slowed down by the introduction of time delay, and the phase angle estimation is also a challenge. While FLL locks the frequency of the power grid instead of the phase angle, FLL is a good way to solve the problem of fast dynamic response. Of course, the main difference between FLL and PLL is the working framework [9].

Generally, FLLs are implemented in the static coordinate system. The function of the prefilter in FLLs is to purify the input signal, which is the same as for the PLLs. In recent years, the research progress of FLL has mainly focused on the design of the prefilter. The most common basic unit of the prefilter is the second-order generalized integrator (SOGI). The FLL based on SOGI (SOGI-FLL) is a nonlinear feedback system, which makes the analysis of SOGI-FLL complicated. Therefore, S. Golestan *et al.* deduced the linear time-periodic

The associate editor coordinating the review of this manuscript and approving it for publication was Ali Raza.

model of extended SOGI-FLL, which could accurately predict the dynamic response and robustness of SOGI-FLL, optimize its performance under weak grid conditions, and provide convenience for further parameter optimization [10], [14]. However, the prediction accuracy is low when the grid is abnormally large, and the result becomes unacceptable.

Based on SOGI, a dual second-order generalized integrator based FLL (DSOGI-FLL) is proposed [11], [15]. The biggest characteristic of DSOGI-FLL is to extract the positive and negative sequence components of the voltage by using the orthogonal signal generated by SOGI. It can also detect the polarity of the voltage under the conditions of harmonics and three-phase imbalance, but the result is still not ideal. To further enhance the filtering ability and improve the accuracy of the SOGI-FLL under harmonically-distorted grid conditions, a solution is to form a decoupling network of multiple SOGIs, which is named MSOGI-FLL. MSOGI-FLL can completely filter out the influence of harmonics, but it will bring the problem of a large amount of computation for the unknown harmonic mode, and it is difficult for each SOGI to select parameters when the tuning frequency is very close [12], [16]. In order to comprehensively improve the harmonic suppression capability of SOGI-FLL under distorted grid conditions, a Comb Filter based FLL (COMB-FLL) is proposed [13], and it can completely eliminate harmonics and DC offset problems under adverse grid conditions. However, this advantage comes at the expense of high memory requirements at high sampling frequencies. The COMB-FLL is implemented by subtracting the delayed signal from the input signal, which inevitably leads to a slow response [13]. In [17], a Comb Filter based on MSOGIs is proposed to quickly and selectively eliminate harmonics while ensuring steady state accuracy, and it removes the complex harmonic decoupling network and reduces the amount of calculation compared with MSOGI-FLL. However, the performance of these SOGI-based FLLs degrades in the presence of noise [1].

Due to the extensive use of nonlinear loads, it is inevitable to increase the harmonics and noise in the power grid [18], [19], such as Radio Frequency Interference, Power Supply Noise, and other electromagnetic interference [20], which will affect the locking frequency ability of the FLL. Active noise cancellation (ANC) is initially used to remove low frequency noise in the field of acoustics and has made remarkable achievements. For example, noise reduction earphones [21], asphalt pavement noise reduction [22], magnetic resonance imaging [23], etc. It is an effective method to counteract the original noise by coming into being with the secondary noise artificially. The basic theory of ANC has been elaborated in [24], and ANC is also widely used in the power field because of its strong adaptability and robustness. Chilipi *et al.* [25] propose an algorithm for basic frequency synchronization using single-phase PLL from ANC. It is also suitable for a grid-connected converter used in distributed generation. This algorithm has adaptive performance under grid frequency fluctuation and voltage distortion. A new ANC harmonic detection method for photovoltaic grid-connected systems was applied in [26]. The results show that the convergence speed of the method is fast and the steady error is small, and the power quality is improved effectively.

To address the issues mentioned above, this paper creatively introduces the ANC, and proposes an enhanced three-phase FLL based on the improved ANC fusion low-pass filters (AL-FLL). Firstly, the ANC algorithm is improved by adding an LPF_2 after $e(n)$ and replacing the original error signal with a $|e_1(n)||e_1(n\text{-}1)|$. Secondly, the function and parameter design of two first-order low-pass filters (LPFs) are explained. In addition, the improved ANC and two first-order LPFs are fused into a prefilter, which is named AL, and the prefiltering technique is implemented in SRF. Using the output frequency feedback loop of FLL, the rotation frequency of the d-q reference frame is regulated in such a way. Furthermore, the principle of AL is elaborated in detail, and the stability of the whole system is analyzed. Finally, the effectiveness of the AL-FLL is further verified by comparative simulation experiments.

II. MODELING ANALYSIS

The structure of AL-FLL is illustrated in Fig. 1. This scheme fuses the improved ANC with the improved S function variable step size least mean square algorithm (I-SVSLMS) and two first-order LPFs into a prefilter instead of simply cascading structure, and the frequency estimation loop is also shown in Fig. 1 for a clear illustration of the implementations.

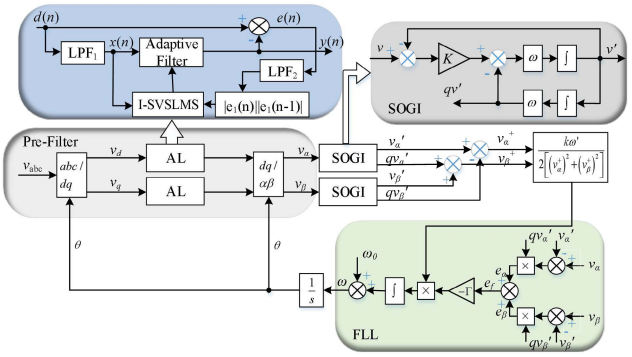

FIGURE 1. Block diagram of AL-FLL.

In Fig. 1, v_{abc} is the input signal with harmonics and noise, and v_d and v_q are the voltage components of the d-axis and q-axis after the input signal passes through the SRF, respectively. ω corresponds to the output frequency of the FLL. In AL, $d(n)$ is the d-axis input signal. $x(n)$ is the input signal of the adaptive filter, which is the output of LPF_1 with the input signal v_d. $\omega(n)$ and $y(n)$ are the adaptive filter weight vector and the output signal after noise reduction, respectively. $e(n)$ is the difference between $d(n)$ and $y(n)$, and $e_1(n)$ is the output signal of LPF_2. In FLL, q is the 90° phase lag factor, qv' signal phase lag v' signal 90°, v_α and v_β mean that signal is converted to α axis and β axis, and e_α and e_β mean frequency error signal on α axis and β axis. Then, the detailed introduction of each part is shown as follows.

A. IMPROVED ACTIVE NOISE CANCELLATION ALGORITHM

The essence of ANC is Wiener filter, whose iteration result is similar to Wiener filter. The difference between ANC and Wiener filter is that ANC can automatically adjust the parameters according to the signal until the result reaches the optimal, while Wiener filter is based on the statistical parameters. The traditional Wiener filter is a method to filter noise signals by taking advantage of the correlation characteristics between stationary processes and spectral characteristics [27]. But in practical application, the previous information about the statistical characteristics of signal and noise can not be obtained in advance, and the calculation amount for estimating the statistical characteristics is relatively massive. In this case, the traditional Wiener filter can not meet the expected requirements, but the ANC has excellent noise reduction performance. For the sake of making ANC more suitable for application in the power field, the algorithm of ANC is modified in this paper.

The improved ANC is composed of a digital filter and an adaptive algorithm. Firstly, it uses an adaptive filter to generate a second signal, which has the same amplitude and opposite phase as the noise in the original signal. Then, using the superposition principle of waves, the output signal of the adaptive filter is superposed with the original input signal to obtain the error signal $e(n)$. Finally, the internal coefficients of the adaptive filter are updated in real time according to the size of the error signal to eliminate the noise. It can be found that if the coefficients of the adjustment filter are not updated in real time, it is just an ordinary filter.

Adaptive algorithms play a crucial role in the performance of the ANC. At present, several kinds of step size algorithms have emerged, like least mean square algorithm (LMS), recursive least square algorithm (RLS), normalization least mean square algorithm (NLMS), normalization variable step size least mean square algorithm (NVSS), S function variable step size least mean square algorithm (SVSLMS) [28], etc. The LMS algorithm has become one of the most widely used algorithms thanks to its simplicity and small amount of computation. The improved kind of LMS algorithm has been widely employed in power systems. The RLS algorithm has quick convergence speed, and its effect is clearly better than the LMS algorithm, but the computational complexity of the RLS algorithm is larger. NLMS is a variable step LMS algorithm, which uses the Euclidean square norm of the input vector to normalize it [29]. The expression of variable step size $\mu(n)$ is:

$$\mu(n) = \frac{\mu_0}{\varepsilon + \| x(n) \|^2} \tag{1}$$

In (1), μ_0 is a constant that is greater than zero, but less than one. ε is a small constant, and is set to prevent (1) from having a denominator of zero when the input signal is zero. The time-varying step solves the contradiction between steady-state error and convergence rate. When the input signal changes abruptly, the step size should be increased to eliminate the disturbance as quickly as possible. But the NLMS algorithm's Euclidean square will grow larger, so that the step size factor can not converge quickly. It indicates that the algorithm has a poor ability to suppress mutation. So as to avoid the difficulty in calculating the step size factor caused by the small value of the input signal, an NVSS algorithm is proposed based on NLMS, which replaces the Euclidean norm of the original input signal with the Euclidean norm of the error square. The expression of variable step size $\mu(n)$ is:

$$\mu(n) = \frac{\mu_0}{1 + \mu_0 \| e(n) \|^2} \tag{2}$$

With the continuous improvement of LMS algorithm, another variable step size algorithm SVSLMS is proposed in [29]. Step size factor $\mu(n)$ is a sigmoid function with error $e(n)$ as parameter, the expression of variable step size $\mu(n)$ is:

$$\mu(n) = \beta\{\frac{1}{1 + \exp(-\alpha|e(n)|)} - 0.5\} \tag{3}$$

When the error is massive within the initial stage, the step size factor increases with the error. However, when the error $e(n)$ is close to zero, the step size factor does not have the characteristic of slow change. To make up for this deficiency, not only is an LPF_2 added after $e(n)$, as shown in Fig. 1, but also a new I-SVSLMS is proposed in this paper. The expression of variable step size $\mu(n)$ of the ANC with I-SVSLMS algorithm is:

$$\mu(\mathrm{n}) = \beta\{1 - \exp[-\frac{1}{2\alpha^2}(|e_1(n)||e_1(n-1)|)]\} \tag{4}$$

In (4), when the error signal $|e_1(n)||e_1(n-1)|$ is near to zero, the step size factor changes slowly. $\mu(n)$ is the step size factor which is related to steady-state error and convergence rate. α is the constant that controls the shape of the function, and β is the constant that controls the range of step coefficients. These two constants which are determined by empirical values of the SVSLMS algorithm. Fig. 2 shows the nonlinear relationship between $e_1(n)$ and $\mu(n)$ in I-SVSLMS.

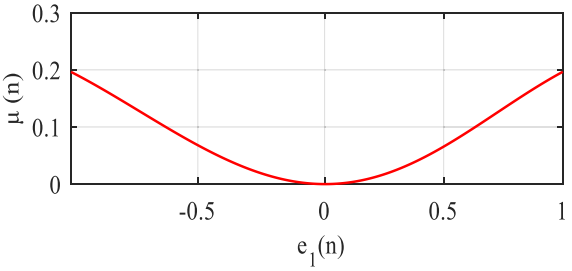

FIGURE 2. The proposed nonlinear relationship between $e_1(n)$ and $\mu(n)$.

To demonstrate the superiority of the I-SVSLMS algorithm, we compared it to the NLMS algorithm, the NVSS algorithm, and the traditional SVSLMS algorithm at different signal to noise ratio (SNR) conditions. The NLMS algorithm and NVSS algorithm adopt fixed step size. The choice of fixed step size is based on the correlation matrix of the input signal and the convergence calculation of optimal value ($\mu = 0.003$) [30]. The I-SVSLMS algorithm and traditional

SVSLMS algorithm adopt optimal parameter values ($\beta = 0.015$, $\alpha = 150$). These parameters are explained in detail in the next section. The order of the adaptive filter is set to 2 and the number of samples is 2000. The reference input signal is a sine wave with an amplitude of 1V and a frequency of 50 Hz. For a clear comparison, Gaussian white noise with SNR of −3dB and −5dB are added on the basis of the reference input signal, respectively. The two signals are mixed as input signals. Different algorithms are used for adaptive filtering of input signals.

The results are shown in Fig. 3(a) and Fig. 3(b), respectively. In Fig. 3, the performance of the algorithm is judged by observing the attenuation rate of the residual noise power, and the simulation results show that the I-SVSLMS algorithm has obvious advantages in convergence speed under different SNR conditions, and the residual noise power (RNP) of I-SVSLMS is minimum. As a result, the improved ANC has excellent noise reduction performance, making it more suitable for use in conditions of voltage distortion and unexpected noise.

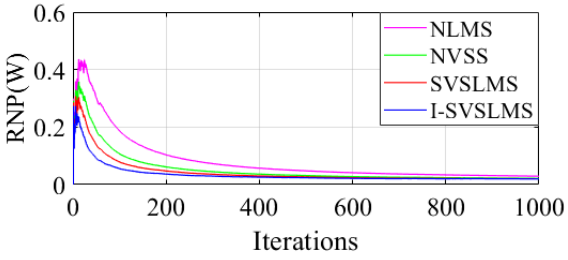

(a) Gaussian white noise with a SNR of -3dB

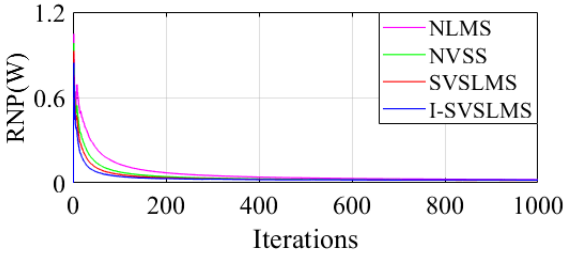

(b) Gaussian white noise with a SNR of -5dB

FIGURE 3. Residual noise power of different algorithms.

B. DESIGN FIRST-ORDER LOW PASS FILTER

As shown in Fig. 1, the AL contains two first-order LPFs, which have different functions. The functions and design methods of the two first-order LPFs are described in detail below.

In general, the ANC has an advantage in dealing with low frequency noise, and LPF_1 is used to filter the high order harmonic and high frequency noise in the SRF to guarantee that the input signal of the improved ANC is a low frequency signal. If the LPF_1 does not exist, the improved ANC will not work properly and this would cause the FLL to be unable to lock the frequency accurately under grid distortion and unexpected noise conditions.

On account of the output frequency of FLL changing greatly in the transient process, the negative sequence components and harmonics in the power grid will cause the problem of high amplitude oscillation of the error signal *e(n)* under the adverse conditions of the power grid. This problem will increase the adjustment time, and it will not even converge. This problem can be easily solved by using LPF_2. However, the LPF_2 requires a very low cut-off frequency to achieve satisfactory accuracy, which slows down the response speed. Since the LPF_1 can filter out some unfavored signals, the cutoff frequency of the LPF_2 can be increased to improve the response speed. The important role of LPF_2 is to purify and reduce the error signal, so as to reduce the number of iterations of the adaptive filter and speed up the response speed.

In order to facilitate the analysis of the LPF_1 input signal characteristics, the three-phase input voltages are assumed to be unbalanced and harmonically distorted, as expressed in (5), where $V_n{}^+(V_n^-)$ and $\theta_n{}^+(\theta_n^-)$ are the amplitude and the phase angle of the nth harmonic component of the positive (negative) sequence of the input voltages, respectively.

$$\begin{aligned} v_a(t) &= \sum_{n=1}^{+\infty}[V_n^+\cos(n\omega t+\theta_n^+)+V_n^-\cos(n\omega t+\theta_n^-)] \\ v_b(t) &= \sum_{n=1}^{+\infty}[V_n^+\cos(n\omega t+\theta_n^+-\frac{2\pi}{3}) \\ &\quad +V_n^-\cos(n\omega t+\theta_n^-+\frac{2\pi}{3})] \\ v_c(t) &= \sum_{n=1}^{+\infty}[V_n^+\cos(n\omega t+\theta_n^++\frac{2\pi}{3}) \\ &\quad +V_n^-\cos(n\omega t+\theta_n^--\frac{2\pi}{3})] \end{aligned} \tag{5}$$

The Park transformation is applied to the three-phase input voltages of (5). The result is:

$$\begin{bmatrix} v_d(t) \\ v_q(t) \end{bmatrix} = T_{dq}\begin{bmatrix} v_a(t) \\ v_b(t) \\ v_c(t) \end{bmatrix} = \begin{bmatrix} v_d^+(t) \\ v_q^+(t) \end{bmatrix} + \begin{bmatrix} v_d^-(t) \\ v_q^-(t) \end{bmatrix} \tag{6}$$

where

$$\begin{aligned} T_{dq} &= \frac{2}{3}\begin{bmatrix} \cos(\widehat{\omega}t+\theta_1^+) & \sin(\widehat{\omega}t+\theta_1^+) \\ -\sin(\widehat{\omega}t+\theta_1^+) & \cos(\widehat{\omega}t+\theta_1^+) \end{bmatrix} \\ &\quad \times\begin{bmatrix} 1 & -\frac{1}{2} & -\frac{1}{2} \\ 0 & -\frac{\sqrt{3}}{2} & -\frac{\sqrt{3}}{2} \end{bmatrix} \end{aligned} \tag{7}$$

$$\begin{bmatrix} v_d^+(t) \\ v_q^+(t) \end{bmatrix} = \begin{bmatrix} \sum_{n=1}^{+\infty} V_n^+\cos[(n\widehat{\omega}-\omega)t+\theta_n^+-\theta_1^+] \\ \sum_{n=1}^{+\infty} V_n^+\sin[(n\widehat{\omega}-\omega)t+\theta_n^+-\theta_1^+] \end{bmatrix} \tag{8}$$

$$\begin{bmatrix} v_d^-(t) \\ v_q^-(t) \end{bmatrix} = \begin{bmatrix} \sum_{n=1}^{+\infty} V_n^- \cos[(n\widehat{\omega}+\omega)t + \theta_n^+ + \theta_1^+] \\ -\sum_{n=1}^{+\infty} V_n^- \sin[(n\widehat{\omega}+\omega)t + \theta_n^+ + \theta_1^+] \end{bmatrix} \tag{9}$$

Under a quasi-locked condition (i.e., $\widehat{\omega} = \omega$), (6) can be rewritten as:

$$\begin{bmatrix} v_d(t) \\ v_q(t) \end{bmatrix} = \begin{bmatrix} v_d^+(t) \\ v_q^+(t) \end{bmatrix} + \begin{bmatrix} v_d^-(t) \\ v_q^-(t) \end{bmatrix} \cong \begin{bmatrix} \overline{v_d} \\ \overline{v_q} \end{bmatrix} + \begin{bmatrix} \widetilde{v_d(t)} \\ \widetilde{v_q(t)} \end{bmatrix} \tag{10}$$

In the SRF, the positive sequence component of the fundamental wave will be transformed to the DC component, and the negative sequence component of the fundamental frequency will be converted to 2nd harmonic components [9]. In general, if the d-q matrix is positively ordered, the positive component will decrease frequency, and the negative component will increase frequency. Therefore, after SRF, the main harmonics in the power grid appear as even harmonics of multiples of 6 (6^{th}, 12^{th}, etc.) [9].

It can be seen from (8) to (10) that the input signal of the LPF_1 has both a DC component and an AC component. Consequently, it is particularly important to select the filter parameters to filter the AC component and retain the DC component to the greatest extent. In [31], the cascade non-adaptive notch filter is used as a prefilter and it is shown that the cascade non-adaptive notch filter's dynamics can be replaced by a simple first-order low pass filter (LPF). Three notch filters with notch frequencies at 2π (100), 2π (300), 2π (600) rad/s and quality factor Q_h is 0.5 [31]. Based on this, the LPF_1 parameters selected in this paper are the simplified first-order LPF of three notch filters, and the transfer function of the LPF_1 is:

$$G(s) = \frac{209}{s + 209} \tag{11}$$

Due to the ability of $LPF_1$to filter out some harmonic components, the cut-off frequency of LPF_2 can be increased to improve response speed. For the convenience of design, the cut-off frequency of the two first-order LPFs is designed to be the same. In this way, the LPF_2 has a high response speed while ensuring accuracy. Fig. 4 shows the Bode diagram of the transfer function of the LPFs. As can be seen in Fig. 4, there is sufficient bandwidth in the low frequency range to ensure that the gain of the DC component is 1.

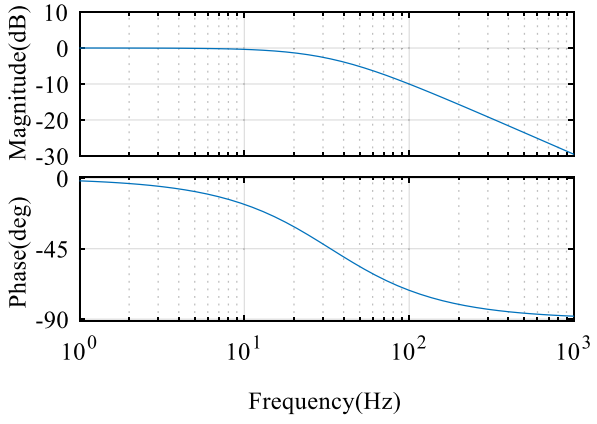

FIGURE 4. Bode diagram of first order low pass filter.

C. FREQUENCY LOCKED LOOP WITH IMPROVED ACTIVE NOISE CANCELLATION FUSED LOW PASS FILTER

Traditional pre-filtering techniques focus on improving FLL performance under power grid imbalance and harmonic distortion conditions, but there has been less research on FLL in the presence of unexpected noise. The noise reduction advantages of the improved ANC and the role of the two LPFs have been described in detail in the previous sector. In this section, the improved ANC and the designed two first-order LPFs are fused into a novel prefilter as shown in Fig. 1.

According to the input signal of LPF_1 analysis, the fundamental component can be extracted by a first-order LPF in a lightly distorted condition. However, the LPF must use a very low cut-off frequency to achieve the ideal filtering effect in the case of severe power grid distortion. The fusion structure between the improved ANC and LPFs was used for noise reduction to avoid degradation of FLL's dynamic response. Taking the d axis as an example, the working principle of AL can be illustrated as follows: The input signal v_d is filtered through the LPF_1, which aims to filter out high order harmonic and high frequency noise, and ensure that the input signal of improved ANC is a low frequency signal. The improved ANC automatically adjusts the step size factor according to the size of the error signal so as to process low-frequency noise. In the processing process, the LPF_2 plays an important role in purifying and reducing the error signal, reducing the number of iterations, and accelerating the convergence speed of the adaptive filter. The improved ANC works with two first-order LPFs to ultimately eliminate external interference.

Park transform has the advantage of decomposing the positive and negative sequence components of the fundamental frequency voltage, and LPF does not introduce any phase shift in the positive sequence voltage. The denoising work of this structure is completed in the SRF, and the estimation frequency of FLL is realized in the static coordinate system. In order to simplify the coordinate system, the output only takes the voltage components of the d-axis and q-axis. The frequency of the SRF is regulated by the output frequency of the FLL. It can be seen from (7) that the rotation frequency is a time-varying value. In general, we use the fundamental frequency of the grid as the rotation frequency. However, the frequency of the input signal is not always fixed or close to the standard value in practical applications, especially in the case of microgrids and weak grids, and the variation of the grid frequency under adverse grid conditions is more likely to be unknown. If the original fundamental frequency is used as the rotation frequency under the unfavorable conditions of

the power grid, the adjusting time of the output frequency signal of the FLL will be increased. This is a good solution by feeding the output frequency of the FLL back to the SRF. Not only does the FLL improve the dynamic response, but also the accuracy of the frequency tracking of the FLL is enhanced. The comparison with or without frequency feedback is described later in the experimental section.

A diagram of FLL can be found in Fig. 1. The improved ANC with two LPFs has been merged into the DSOGI-FLL. The working principle of DSOGI-FLL has been expounded in detail in [11] and [12]. DSOGI-FLL provides the fundamental component and its orthogonal component of the input voltage. The positive and negative sequence components of the grid voltage that are independent of each other can be obtained by the normalization of the FLL gain. The estimated grid frequency can be obtained by adjusting the product of e_f and FLL gain normalization through the integral controller. According to the gain normalization of FLL, the DSOGI-FLL system can be simplified into a first-order linearized frequency adaptive system, and the transfer function is:

$$\frac{\omega_2}{\omega_1} = \frac{\Gamma}{s+\Gamma} \tag{12}$$

where ω_1 is the frequency of the input signal, ω_2 is the resonant frequency of SOGI, Γ is the loop gain, and the estimated adjustment time is t_s [11]. The estimated value of adjustment time is:

$$t_s \approx \frac{4.6}{\Gamma} \tag{13}$$

To verify the harmonic suppression ability of AL. Fig. 5 shows the output voltage waveform of AL when the grid voltage with a frequency of 50Hz and a voltage amplitude of 311V is subjected to 30% zero-sequence 3^{rd} harmonics, 10% negative sequence 5^{th} harmonics, 10% positive sequence 7^{th} harmonics and 5% negative sequence 11^{th} harmonics, respectively. To better see the effect of AL on each harmonic, the harmonic voltages are added in turn. Fig. 5(a) is the three-phase voltage input signal with harmonics and noise, and Fig. 5(b) is the three-phase output voltage waveform after the denoising of AL. In Fig. 5(b), the output voltage quickly reaches the fundamental frequency amplitude in the case of harmonic injection, indicating that the dynamic response of the AL is very fast. By comparing the voltage waveform in Fig. 5(a) and Fig. 5(b), it can be seen that the voltage signal after AL denoising has no attenuation in amplitude and no change in frequency when it reaches a steady state, indicating that AL has a strong ability to suppress various harmonics. The total harmonic content of FFT output voltage is shown in Fig. 5(c), and the total harmonic content is only 0.24%. Obviously, the AL performs well in terms of noise reduction.

It is important to clarify that the fusion of the improved ANC and first-order LPFs technology is to enhance the noise reduction performance of FLL under the condition of grid distortion. In addition, the AL-FLL structure proposed in this paper is a FLL suitable for three-phase systems, which is more universal than single-phase.

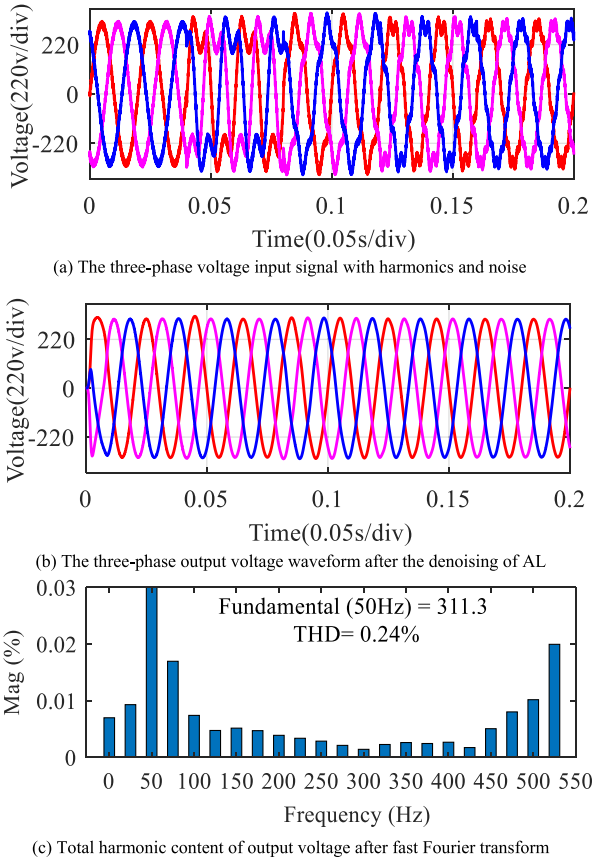

(a) The three-phase voltage input signal with harmonics and noise

(b) The three-phase output voltage waveform after the denoising of AL

(c) Total harmonic content of output voltage after fast Fourier transform

FIGURE 5. The performance of AL under harmonically distorted gird condition.

III. STABILITY ANALYSIS AND PARAMETER SELECTION

The AL-FLL proposed in this paper should not only ensure the simplicity of calculation, but also consider stability. Due to the non-linearity of the adaptive filter, it cannot be proved by traditional methods. In this section, the stability analysis is illustrated in two parts, and one is the AL and the other is the FLL.

According to Fig. 1 in Section II, we can get the following expression.

$$x(n) = d(n) * h_1(n) \tag{14}$$

$$e_1(n) = e(n) * h_2(n) \tag{15}$$

where * represents convolution, and $d(n)$ is the d-axis input signal.

The expression of $y(n)$ is:

$$y(n) = w(n)x^T(n) \tag{16}$$

The expression of $e(n)$ is:

$$e(n) = d(n) - y(n) \tag{17}$$

In order to facilitate stability analysis, this paper simplifies the first-order low-pass filter to a pure delay link [32]. The expression in the Z domain is:

$$H_1(z) = z^{-k_1} \tag{18}$$

$$H_2(z) = z^{-k_2} \tag{19}$$

where k_1 and k_2 are time delays. $e_1(n)$ is the output signal after the error signal has been passed through the $h_2(n)$. The expression of $e_1(n)$ is:

$$\begin{aligned} e_1(n) &= [d(n) - x^T(n)w(n)] * h_2(n) \\ &= d(n-k_2) - x^T(n-k_2)w(n-k_2) \end{aligned} \tag{20}$$

In order to find the best weight vector of filter, a criterion is set first. The most commonly used criterion is the minimum mean square error criterion [32], because the advantage of this principle is that it is simple in theoretical analysis. The objective function obtained by the steepest descent method is:

$$\begin{aligned} H(n) &= E[e_1^2(n)] \\ &= E[d^2(n-k_2)] - 2P^T w(n-k_2) \\ &\quad + w^T(n-k_2)Rw(n-k_2) \end{aligned} \tag{21}$$

where $P=E[d(n\text{-}k_2)x(n\text{-}k_2)]$, $R=E[x(n\text{-}k_2)x^{\mathrm{T}}(n\text{-}k_2)]$.

For stationary input signals, $H(n)$ is a quadratic function of the weight vector. Because R is a positive definite symmetry, it shows that there is a unique minimum value of $H(n)$. According to the recursive rule, the weight vector at the next moment is equal to the current weight vector minus a change proportional to the weight vector gradient. The expression of $w(n)$ is:

$$w(n+1) = w(n) - \mu\nabla(n) \tag{22}$$

where the gradient $\nabla(n)$ is:

$$\nabla(n) = \frac{\partial H(n)}{\partial w(n)} = -2p + 2RW \tag{23}$$

Let $\frac{\partial H(n)}{\partial w(n)} = 0$, then the expression of the optimal weight loss is:

$$w_0 = R^{-1}P \tag{24}$$

$$\nabla(n) = -2(P - Rw(n-k_2)) \tag{25}$$

Combined with the above formulas (21), (23) and (24), then the iterative formula of weight loss is:

$$w(n+1) = w(n) - 2\mu R[w(n-k_2) - w_0] \tag{26}$$

Because R is the autocorrelation matrix of the input signal of the filter, and it is a symmetric positive definite quadratic matrix, it can be transformed into the standard form by orthogonal transformation, and the expression of R is:

$$R = Q^T \Lambda Q \tag{27}$$

where Q is orthogonal matrix, Λ is the diagonal matrix of eigenvalues of R autocorrelation matrix.

Let $V(n) = w(n)\text{-}w_0$. After the Q matrix linearly transforms $V(n)$. Then (25) can be rewritten as:

$$V(n+1) = V(n) - 2\mu RV(n-k_2) \tag{28}$$

If both sides of the above formula are multiplied by Q^{-1}, the expression is:

$$V'(n+1) = V'(n) - 2\mu\Lambda V(n-k_2) \tag{29}$$

Transform (29) into scalar form, then the expression of the i component is:

$$v_i'(n+1) = v_i'(n) - 2\mu\lambda_i v_i'(n-k_2) \tag{30}$$

Z transformation is carried out on both sides of (30), and the expression after consolidation is:

$$v_i'(z) = \frac{z^{k_2+1}v_i'(0)}{z^{k_2+1} - z^{k_2} + 2\mu\lambda_i} \tag{31}$$

If the system is to be stable, the poles of $v_i'(z)$ should be in the unit circle of Z plane, and that is:

$$f(z) = z^{k_2+1} - z^{k_2} + 2\mu\lambda_i \tag{32}$$

Using the root locus method to analyze the change of the roots for $f(z)$, it can be found that the necessary and sufficient condition for the system to remain stable is [33].

$$0 < \mu < \frac{1}{\lambda_{\max}} \sin\frac{\pi}{2(2k_2+1)} \tag{33}$$

where λ_{max} is the maximum eigenvalue of the input signal autocorrelation matrix [29].

From (33), we can see that the step factor is related to the eigenvalue and the size of the delay. In order to ensure the convergence of the I-SVSLMS algorithm, the range of step size factor should be determined. As we all know, the step factor of the Least mean square algorithm is $0 < \mu < 1/\lambda_{max}$. In (4), the step size factor is also limited by the error signal. Since the absolute value of ranges from 0 to infinity, the exponential range of exp is 0 to 1, and the value range of step size factor can be obtained as shown in (34).

$$0 < \mu < \beta \sin\frac{\pi}{2(2k_2+1)} \tag{34}$$

The time delay is related to the cut-off frequency of the LPF. The transfer function of LPF_2 can be regarded as a first order damp elements and its time constant is approximately k_2. $k_2$is approximately 0.00478 according to (11). After substituting this value into (34), the step size factor of the I-SVSLMS algorithm is $0 < \mu < \beta$ *(i.e.,* $\beta = 0.015$*)*. The β parameter is explained later. The step size factor in this range can ensure the stability of AL.

In Section II, it has been shown that DSOGI-FLL can be simplified into a first-order linear frequency adaptive system, whose transfer function is (12), and whose stability time can be approximated by (12). In this paper, k is set as $\sqrt{2}$ and Γ is set as 150 to achieve a stable time of 30ms [2]. From (12), the characteristic equation of DSOGI-FLL can be deduced. i.e., (35).

$$D(s) = s + 2\Gamma \tag{35}$$

Obviously, the coefficients of the characteristic equation of DSOGI-FLL are all positive. The FLL is stable as indicated by the Hurwitz criterion.

The AL-FLL structure is the product of linear and nonlinear combinations. As long as the value range of the step size factor is guaranteed, the improved ANC is stable. Since the

transformation matrix is bounded when the output frequency changes, from the external characteristics of AL, a finite input signal has a finite output. From the above analysis, it can be seen that both AL and DSOGI-FLL are stable. In addition, due to the cascade structure relationship between the prefilter and the FLL, the prefilter and the FLL depend on a bounded frequency interaction, so the whole system is stable.

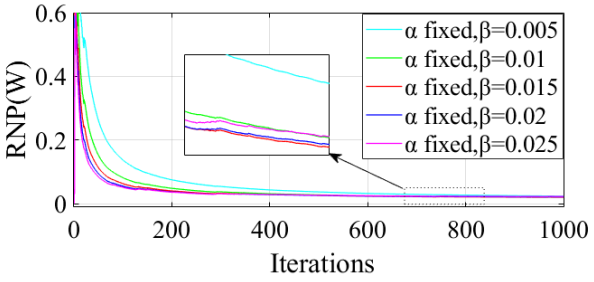

FIGURE 6. The effect of different β on the performance of adaptive filtering.

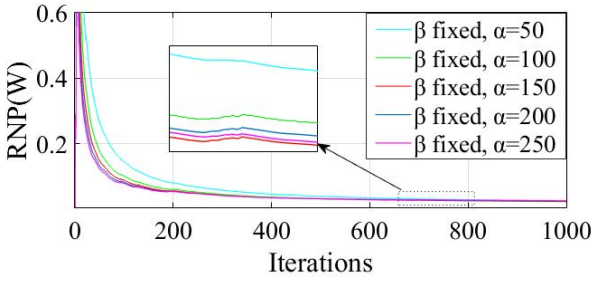

FIGURE 7. The effect of different α on the performance of adaptive filtering.

Since the stability of AL-FLL is related to the size of β, this paper uses genetic algorithm to optimize it. Genetic algorithm has the ability to identify the optimal value. Residual noise power is improved as a fitness function. The β experience values range from 0.001 to 0.1. Elite count was set as 2 and cross over fraction 0.8 [34]. The scale and shrink parameters which decide the standard deviation of the Gaussian distribution used in the Gaussian mutation function was set as 1. In Fig. 6, the best value of β is taken to be 0.02 and this β guarantees faster convergence under large error conditions and the lowest residual noise power into the steady state. Fig. 7 shows the effect of different α values on the adjustment time and steady-state effect of adaptive filtering. The results of 30 independent simulations were statistically averaged. After several analyses and comparisons of residual noise reduction rates and residual noise content, $\beta = 0.015$ and $\alpha = 150$ are finally selected.

IV. EXPERIMENTAL RESULT

In order to verify the theoretical analysis above and the correctness of the proposed method, an experimental platform was set up. A Programmable AC Power (TPA-200) supply is used in this experiment, and the DC-link voltage is provided by the DC power supply NHWY500-3. The AL-FLL is

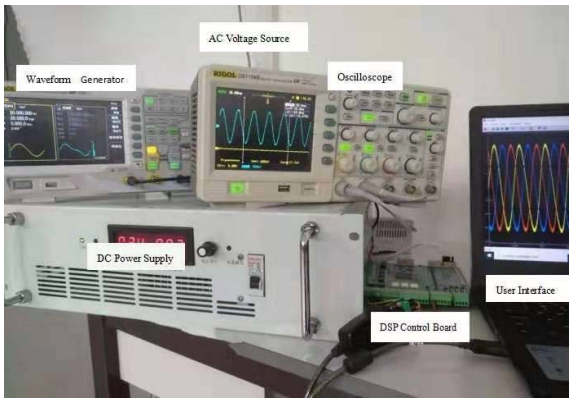

FIGURE 8. Experimental platform.

realized by the TMS320F28335 digital signal processor R&D board. The experimental platform is shown in Fig. 8. In this section, the experimental and analysis results of the AL-FLL are given in detail.

In this experiment, the setting voltage is 50 Hz, and the sampling frequency is fixed at 10 kHz. The structure AL-FLL proposed in this paper is compared with the AL-FLL without frequency ω feedback (AL-NF-FLL), standard SOGI-FLL and COMB-FLL, respectively. Seven test conditions (Voltage sag, Voltage swell, harmonically-distorted grid conditions, Phase angle jump with harmonics injection, Phase angle jump under distorted grid conditions, frequency step with harmonics injection, and frequency step under distorted grid conditions) were designed to analyze the dynamic response and steady-state performance of AL-FLL.

SOGI-FLL is one of the comparisons to the FLLs due to its fast response speed. The COMB-FLL is designed on the basis of SOGI-FLL, which enhances the anti-jamming ability, so as to compare its anti-jamming ability with AL-FLL. Considering that the fundamental frequency in the grid is time-varying, the AL-FLL is also compared with the AL-NF-FLL. In order to more accurately and intuitively evaluate the performance of AL-FLL, we compared AL-FLL with SOGI-FLL, COMB-FLL and AL-NF-FLL under the same experimental conditions. For SOGI-FLL, filter gain k is $\sqrt{2}$ and $\Gamma = 150$ [12], [13]. For COMB-FLL, $k = 4/\pi$ and $\Gamma = 160$ [13]. The parameter selection of AL-FLL and AL-NF-FLL is the same as that of SOGI-FLL.

The experimental result of the AL-FLL during voltage disturbance is compared with that of SOGI-FLL, COMB-FLL and AL-NF-FLL in Fig. 9. In the experiment, the grid voltage first dropped to 70% of the nominal voltage, and then rose to 130% of the nominal voltage. These two situations correspond to the experimental conditions of voltage sag and voltage swell, respectively. In the case of voltage sag, the experiment results can be observed that the SOGI-FLL and COMB-FLL have 1% settling time (i.e., the time after which the frequency error reaches and remains within 0.5 Hz of its final value) of around 0.85 cycle and 0.625 cycle with a peak frequency deviation of 0.77 Hz and 0.72Hz, respectively.

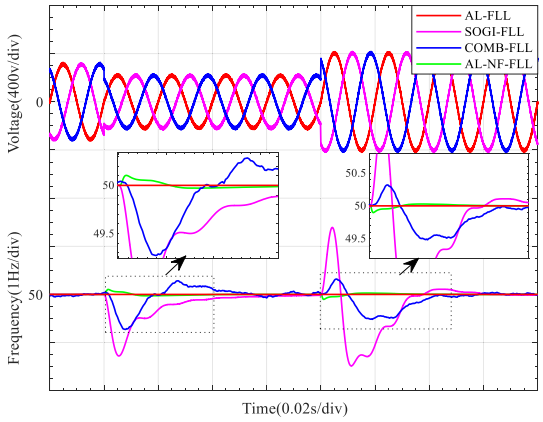

FIGURE 9. Comparison results between different FLLs under voltage sag and Voltage swell.

Meanwhile, when the voltage swells, the 1% settling time of the SOGI-FLL and COMB-FLL is about 1.55 cycles, and the peak frequency deviation is 1.4 Hz and 0.5 Hz respectively. However, the peak frequency deviation of the proposed AL-FLL and AL-NF-FLL is less than 0.1 Hz. It can be seen that the introduction of ANC enhances the robustness of the FLL against voltage interference. Because the AL-FLL has output frequency feedback, its peak overshoot is less than that of the AL-NF-FLL, and its frequency estimation is more accurate.

The noise reduction performance of AL has been proved in the previous section. This experiment aims to prove the superiority of AL-FLL under harmonic conditions. Fig. 10 shows the result of AL-FLL and other FLLs under the harmonic injection. The grid voltage parameters in this experiment are $V_1 = 1$ $(p.u.)$, $V^-_1 = 0.1$ $(p.u.)$, $V^0_3 = 0.3$ $(p.u.)$, $V^-_5 = V^+_7 = 0.1$ $(p.u.)$ and $V^-_{11} = 0.05$ $(p.u.)$. From the experimental results, AL-FLL and AL-NF-FLL can quickly eliminate the influence of harmonics. The peak overshoot was 0.1Hz, and the response time was 0.5 cycles. While the response time of the COMB-FLL is about 0.9 cycles, and the peak frequency deviation is 0.2 Hz. The frequency error

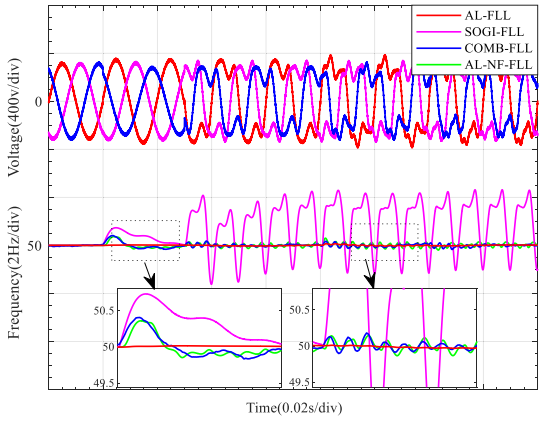

FIGURE 10. Comparison results between different FLLs under harmonically-distorted gird condition.

at nearly 2Hz on the SOGI-FLL has become unacceptable. Thanks to the AL prefilter has a good ability to suppress harmonics, the frequency overshoot of AL-FLL and AL-NF-FLL can be ensured to be small overshoot and short adjustment time. In addition, because AL-FLL has frequency feedback, there is no frequency deviation during Park transformation, and the fundamental wave component can be completely converted into DC, so AL-FLL has a better harmonic suppression ability than AL-NF-FLL.

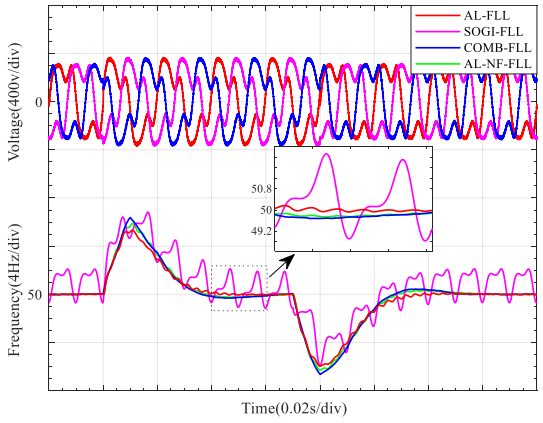

FIGURE 11. Comparison results between different FLLs under 40° phase angle jump with harmonics.

To verify the working ability of AL-FLL under the condition of three-phase unbalance, two sets of experiments were set for phase angle jump of 40° and frequency step change of 5Hz in the Zero order third harmonic and negative order fifth harmonic injection environment ($V_1 = 1$ $(p.u.)$, $V^0_3 = 0.3$ $(p.u.)$, $V^-_5 = 0.1$ $(p.u.)$), respectively. Fig. 11 shows the response results of AL-FLL and other FLLs under a phase angle jump of 40°. It can be seen that the AL-FLL has a 1% settling time of around 1.6 cycles, compared to 1.7 cycles of AL-NF-FLL, 2 cycles of COMB-FLL and 2.35 cycles of SOGI-FLL. The peak frequency is measured at 5.2Hz, 5.6Hz, 6.3Hz and 6.82Hz respectively. Moreover, with the increase in the superposition of harmonic types, the peak overshoot and adjustment time of FLL have been also increased. In Fig. 12, the result of the AL-FLL during a step change in frequency (5Hz) is compared to that of the SOGI-FLL, COMB-FLL, and AL-NF-FLL. It can be observed that the COMB-FLL and AL-NF-FLL have 1% settling time of about 2.1 cycles and 1.9 cycles with a peak frequency deviation of 0.42 Hz and 0.39 Hz, respectively. Although SOGI-FLL has good dynamic characteristics, the output frequency fluctuates nearly 2.5Hz under the frequency step change condition. The frequency errors cannot meet the requirements of the grid connection. However, the AL-FLL has only a 1% settling time of around 1.4 cycles without peak overshoot. Compared with other FLLs, the adjustment time and overshoot of AL-FLL are perfect. The steady-state error is also minimal when the steady-state is reached.

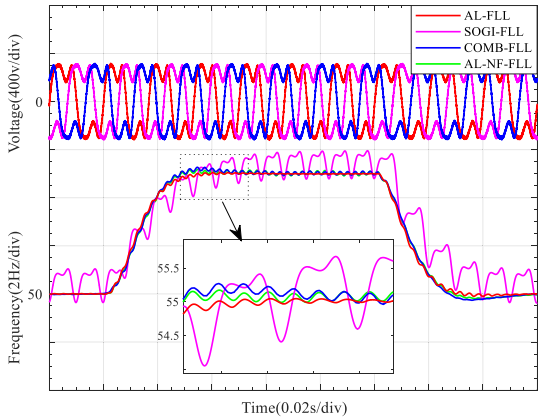

FIGURE 12. Comparison results between different FLLs under 5Hz frequency step with harmonics.

Obviously, AL-FLL has strong anti-jamming ability, which ensures rapidity and the best accuracy.

To sum up, the steady state error and dynamic response of AL-FLL were studied by designing experiments under seven working conditions. For intuitive comparison, the response time obtained with SOGI-FLL, COMB-FLL, AL-NF-FLL and AL-FLL under different test conditions are summarized in Table 1. The experimental results show that the AL-FLL has strong anti-interference ability, smaller steady-state errors, faster dynamic response speed and more accurate frequency locking ability compared with the above three kinds of FLLs. In order to facilitate the comparison of the computational complexity of FLLs, Table 2 gives a detailed description by numerical operation.

The purpose of this paper is to propose a new structure of AL-FLL to solve the problem of SOGI-based FLLs descending in the case of noise. Due to the unique anti-jamming design of AL, the adjustment time can be effectively reduced, so that the frequency can be locked more quickly. AL-FLL takes advantage of the noise reduction capability of AL to improve the performance of FLL under the conditions of grid distortion and noise, which is relatively easy to implement in hardware. At the same time, the output frequency of the FLL is used to update the rotation frequency of SRF in real time, which ensures that the FLL has an accurate output frequency.

It is important to clarify that all the pre-filtering of FLLs in this paper is carried out in d-q coordinates, so that the comparison can be consistent. Since SOGI-FLL is mainly used in single-phase systems, the calculation cost in Table 2 is compared with that in single-phase systems for fair comparison. It can be seen from the Table 2 that AL-FLL has little difference in computational complexity with other FLLs, but it is far superior to other FLLs in performance.

Since frequency and phase angle are necessary for power grid synchronization and inverter control system in three-phase imbalance [10]. The phase angle estimation is given in this paper under the condition that the phase angle changes 20° and the frequency changes 10Hz. All phase angle values

TABLE 1. Comparision the advanced FLLS and AL-FLL.

Aspects (1% settling time) [a]	AL-FLL	SOGI-FLL	COMB-FLL	AL-NF-FLL
Voltage sag (V_1 = 0.7 (p.u.)) Peak frequency deviation	Almost unaffected [b] 0.06Hz	17ms 0.77Hz	12ms 0.72Hz	Almost unaffected 0.1Hz
Voltage swell (V_1 = 1.3 (p.u.)) Peak frequency deviation	Almost unaffected 0.06Hz	30ms 1.4Hz	30ms 0.5Hz	Almost unaffected 0.1Hz
40° Phase angle jump with harmonics injection (V^0_3 = 0.3 (p.u.), V^-_5 =0.1 (p.u.)) Peak frequency deviation	35ms 5.2Hz	48ms 6.82Hz	40ms 6.3Hz	36ms 5.6Hz
-40° Phase angle jump under distorted grid conditions (V^0_3 = 0.3 (p.u.), V^-_5 =0.1 (p.u.)) Peak frequency deviation	36ms 5.2Hz	62ms 6.83Hz	42ms 6.3Hz	38ms 5.6Hz
5 Hz frequency step with harmonics injection (V^0_3 = 0.3 (p.u.), V^-_5 =0.1 (p.u.)) Peak frequency deviation	26ms 0Hz	59ms 2.4Hz	38ms 0.42Hz	25ms 0.39Hz
-5 Hz frequency step under distorted grid conditions (V^0_3 = 0.3 (p.u.), V^-_5 =0.1 (p.u.)) Peak frequency deviation	25ms 0Hz	57ms 2.41Hz	40ms 0.41Hz	25ms 0.38Hz
Harmonic rejection capability (V_1 = 1 (p.u.), V^-_1 = 0.1 (p.u.), V_3 =0.3 (p.u.), V_5 = V_7 = 0.1 (p.u.) V_{11} =0.05 (p.u.))	Excellent	Poor	Good	Good

TABLE 2. Computational cost of the FLLS.

FLL NAME	×&±[1]	sin &cos	÷	Stored Sample[2]
SOGI-FLL	10	0	2	0
COMB-FLL[3]	10	2	3	T/T_s
AL-FLL	12	2	3	0
AL-NF-FLL	12	2	3	0

[1] Multiply, devision, add, and subtract numbers in a single run.
[2] Sin&cos represents the operation in d-q coordinate transformation. Stored samples column does not include the required samples for the digital implementation of states (integrators). T denotes a cycle of the fundamental frequency.
[3] The computational cost of the COMB-FLL does not include the required operations for realizing a variable-length fractional delay. The prefiltering of COMB-FLL is performed in d-q coordinates.

are calculated according to the following equations [10].

$$\theta^+ = \tan^{-1}\frac{v^+_\beta}{v^+_\alpha} \tag{36}$$

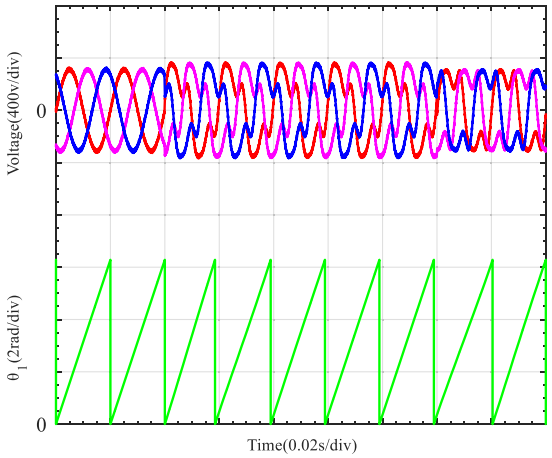

FIGURE 13. Response of the AL-FLL with 20° phase angle jump ($\theta_1 = \theta^+$).

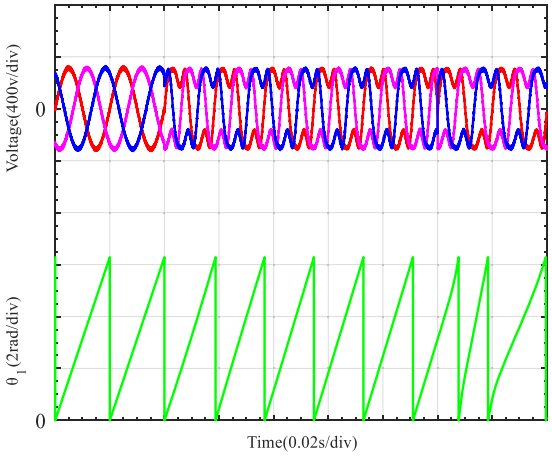

FIGURE 14. Response of the AL-FLL with 10 Hz frequency changes ($\theta_1 = \theta^+$).

Fig. 13 shows the phase angle estimate under 20° phase angle jump with harmonics injection ($V_1 = 1$ $(p.u.)$, $V^0{}_3 = 0.3$ $(p.u.)$, $V^-{}_5 = 0.1$ $(p.u.)$). When the phase angle of the input voltage jumps by 20°, the estimated phase angle will also lead and the original phase angle can be quickly restored.

Fig. 14 shows the phase angle estimate under 10 Hz frequency step change with harmonics injection ($V_1 = 1$ $(p.u.)$, $V^0{}_3 = 0.3$ $(p.u.)$, $V^-{}_5 = 0.1$ $(p.u.)$). It can be seen that AL-FLL has good performance in phase angle estimation.

V. CONCLUSION

A new FLL named AL-FLL is proposed, and AL-FLL differs from other FLLs in that ANC is introduced into the prefilter to solve the grid distortion and noise problems.

Firstly, a new prefiltering structure of AL-FLL is proposed which is fused by the improved ANC and two first-order LPFs. Improved ANC is based on the SVSLMS algorithm, and a new calculation method for the ANC's step size factor is proposed. Secondly, the functions of two LPFs are described in detail, and the parameter selection of two LPFs based on the input signal under SRF is also given. At last, the stability of the whole system is illustrated in two parts. One is the AL according to the root locus method and the other is the FLL using the Hurwitz criterion.

The experimental results show that the AL-FLL has strong anti-interference ability, smaller steady-state errors, faster dynamic response speed and more accurate frequency locking ability compared with SOGI-FLL, COMB-FLL and AL-NF-FLL. It has a more extensive application prospect in the electric power field.

REFERENCES

[1] H. Ahmed, S. Biricik, and M. Benbouzid, "Linear Kalman filter-based grid synchronization technique: An alternative implementation," *IEEE Trans. Ind. Informat.*, vol. 17, no. 6, pp. 3847–3856, Jun. 2021.

[2] W. Ma, S. Ouyang, and W. Xu, "Improved frequency locked loop based synchronization method for three-phase grid-connected inverter under unbalanced and distorted grid conditions," *Energies*, vol. 12, no. 6, p. 1023, Mar. 2019.

[3] A. K. Dubey, J. P. Mishra, and A. Kumar, "Performance improvement of shunt active power filter under variable grid frequency condition using complex coefficient filter-frequency locked loop," *Int. J. Circuit Theory Appl.*, vol. 49, no. 4, pp. 1164–1181, Apr. 2021.

[4] S. Murugesan and V. Murali, "Hybrid analyzing technique based active islanding detection for multiple DGs," *IEEE Trans. Ind. Informat.*, vol. 15, no. 3, pp. 1311–1320, Mar. 2019.

[5] J. Yu, W. Shi, J. Li, L. Deng, and M. Pei, "A discrete-time non-adaptive SOGI-based frequency-locked loop," *IEEE Trans. Power Syst.*, vol. 35, no. 6, pp. 4912–4915, Nov. 2020.

[6] S. Golestan, M. Monfared, and F. D. Freijedo, "Design-oriented study of advanced synchronous reference frame phase-locked loops," *IEEE Trans. Power Electron.*, vol. 28, no. 2, pp. 765–778, Feb. 2013.

[7] C. Liu, J. Jiang, J. Jiang, and Z. Zhou, "Enhanced grid-connected phase-locked loop based on a moving average filter," *IEEE Access*, vol. 8, pp. 5308–5315, 2020.

[8] D. G. Abhilash Krishna and A. Karthikeyan, "Design and analysis of frequency adaptive CDSC-PLL for dynamic voltage restorer during adverse grid conditions," in *Proc. IEEE Int. Conf. Power Electron., Smart Grid Renew. Energy (PESGRE)*, Jan. 2020, pp. 1–5.

[9] P. Kanjiya, V. Khadkikar, and M. S. E. Moursi, "A novel type-1 frequency-locked loop for fast detection of frequency and phase with improved stability margins," *IEEE Trans. Power Electron.*, vol. 31, no. 3, pp. 2550–2561, Mar. 2016.

[10] S. Golestan, J. M. Guerrero, and J. C. Vasquez, "Modeling and stability assessment of single-phase grid synchronization techniques: Linear time-periodic versus linear time-invariant frameworks," *IEEE Trans. Power Electron.*, vol. 34, no. 1, pp. 20–27, Jan. 2019.

[11] S. Ouyang, W. Ma, and Q. Ke, "A multi-resonant decoupling network synchronization method based on improved DSOGI-FLL for grid connected converter," *Automat. Electr. Power Syst.*, vol. 42, no. 19, pp. 133–139, Oct. 2018.

[12] P. Rodriguez, A. Luna, I. Candela, R. Mujal, R. Teodorescu, and F. Blaabjerg, "Multiresonant frequency-locked loop for grid synchronization of power converters under distorted grid conditions," *IEEE Trans. Ind. Electron.*, vol. 58, no. 1, pp. 127–138, Jan. 2011.

[13] H. Liu, Y. Xing, and H. Hu, "Enhanced frequency-locked loop with a comb filter under adverse grid conditions," *IEEE Trans. Power Electron.*, vol. 31, no. 12, pp. 8046–8051, Dec. 2016.

[14] S. Golestan, J. M. Guerrero, J. C. Vasquez, A. M. Abusorrah, and Y. Al-Turki, "Standard SOGI-FLL and its close variants: Precise modeling in LTP framework and determining stability region/robustness metrics," *IEEE Trans. Power Electron.*, vol. 36, no. 1, pp. 409–422, Jan. 2021.

[15] Q. Yan, R. Zhao, X. Yuan, W. Ma, and J. He, "A DSOGI-FLL-based dead-time elimination PWM for three-phase power converters," *IEEE Trans. Power Electron.*, vol. 34, no. 3, pp. 2805–2818, Mar. 2019.

[16] L. H. Meneghetti, E. L. Carvalho, E. G. Carati, J. P. da Costa, C. M. de Oliveira Stein, and R. Cardoso, "Energy storage system for programmable dispatch of photovoltaic generation," in *Proc. 21st Eur. Conf. Power Electron. Appl. (EPE ECCE Europe)*, Genova, Italy, Sep. 2019, p. 10.

[17] C. Xie, K. Li, J. Zou, K. Zhou, and J. M. Guerrero, "Multiple second-order generalized integrators based comb filter for fast selective harmonic extraction," in *Proc. IEEE Appl. Power Electron. Conf. Expo. (APEC)*, Mar. 2019, pp. 2427–2432.
[18] F. Blaabjerg, R. Teodorescu, M. Liserre, and A. V. Timbus, "Overview of control and grid synchronization for distributed power generation systems," *IEEE Trans. Ind. Electron.*, vol. 53, no. 5, pp. 1398–1409, Oct. 2006.
[19] R. M. Santos Filho, P. F. Seixas, P. C. Cortizo, L. A. B. Torres, and A. F. Souza, "Comparison of three single-phase PLL algorithms for UPS applications," *IEEE Trans. Ind. Electron.*, vol. 55, no. 8, pp. 2923–2932, Aug. 2008.
[20] J. Wu, Q. Guo, C. Yue, L. Xie, and C. Zhang, "Special electromagnetic interference in the ionosphere directly correlated with power system," *IEEE Trans. Electromagn. Compat.*, vol. 62, no. 3, pp. 947–954, Jun. 2020.
[21] S. M. Kuo, S. Mitra, and W.-S. Gan, "Active noise control system for headphone applications," *IEEE Trans. Control Syst. Technol.*, vol. 14, no. 2, pp. 331–335, Mar. 2006.
[22] H. Zhang, Z. Liu, and X. Meng, "Noise reduction characteristics of asphalt pavement based on indoor simulation tests," *Construct. Building Mater.*, vol. 215, pp. 285–297, Aug. 2019.
[23] G. Sun, "*In-situ* adaptive speech enhancement using directional microphone applied to magnetic resonance imaging," in *Proc. Inter-Noise Noise-Con Congr. Conf.*, 2015, pp. 1001–1009.
[24] S. Luo and Z. Hou, "An adaptive detecting method for harmonic and reactive currents," *IEEE Trans. Ind. Electron.*, vol. 42, no. 1, pp. 85–89, Feb. 1995.
[25] R. R. Chilipi, N. Al Sayari, A. R. Beig, and K. Al Hosani, "A multitasking control algorithm for grid-connected inverters in distributed generation applications using adaptive noise cancellation filters," *IEEE Trans. Energy Convers.*, vol. 31, no. 2, pp. 714–727, Jun. 2016.
[26] Z. Li, L. Wang, Y. Wang, and G. Li, "Harmonic detection method based on adaptive noise cancellation and its application in photovoltaic–active power filter system," *Electr. Power Syst. Res.*, vol. 184, Jul. 2020, Art. no. 106308.
[27] M. Badoni, A. Singh, and B. Singh, "Comparative performance of Wiener filter and adaptive least mean square-based control for power quality improvement," *IEEE Trans. Ind. Electron.*, vol. 63, no. 5, pp. 3028–3037, May 2016.
[28] Z. Yuan and X. Songtao, "New LMS adaptive filtering algorithm with variable step size," in *Proc. Int. Conf. Vis., Image Signal Process. (ICVISP)*, Osaka, Japan, Sep. 2017, pp. 1–4.
[29] S. Haykin, *Adaptive Filter Theory*, 3rd ed. Upper Saddle River, NJ, USA: Prentice-Hall, 1996.
[30] Y. Chen, J. Tian, and Y. Liu, "Variable step size LMS algorithm based on modified sigmoid function," in *Proc. Int. Conf. Audio, Lang. Image Process.*, Shanghai, China, Jul. 2014, pp. 627–630.
[31] J. Ni and F. Li, "Adaptive combination of subband adaptive filters for acoustic echo cancellation," *IEEE Trans. Consum. Electron.*, vol. 56, no. 3, pp. 1549–1555, Aug. 2010.
[32] H. Khazraj, F. F. da Silva, C. L. Bak, and S. Golestan, "Analysis and design of notch filter-based PLLs for grid-connected applications," *Electric Power Syst. Res.*, vol. 147, pp. 62–69, Jun. 2017.
[33] I. Tabatabaei Ardekani and W. H. Abdulla, "Theoretical convergence analysis of FxLMS algorithm," *Signal Process.*, vol. 90, no. 12, pp. 3046–3055, Dec. 2010.
[34] B. Paul and P. Mythili, "ECG noise removal using GA tuned sign-data least mean square algorithm," in *Proc. IEEE Int. Conf. Adv. Commun. Control Comput. Technol. (ICACCCT)*, Aug. 2012, pp. 100–103.

LEI PAN received the Ph.D. degree from the Hebei University of Technology, Tianjin, China, in 2014. He is currently an Associate Professor with Tianjin Chengjian University, Tianjin. His research interests are power converters and renewable energy generation.

ZHEN LI received the B.S. degree from the Hebei University of Technology City College, Tianjin, China, in 2018. He is currently pursuing the master's degree with Tianjin Chengjian University, Tianjin. His research interests include power converters and renewable energy generation.

JINGMEI ZHANG received the Ph.D. degree from Southeast University, Nanjing, China, in 2014. She is currently a Lecturer with Tianjin Chengjian University, Tianjin, China. Her research interests include nonlinear control and power converters modulation.

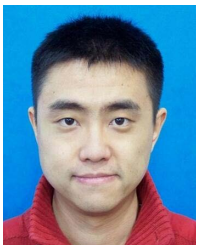

YI PANG received the Ph.D. degree from Nankai University, Tianjin, China, in 2015. He is currently a Lecturer with Tianjin Chengjian University, Tianjin. His research interests include power converter systems and electrical motor drives.